High-Resolution and Accurate RV Map Estimation by Spare Bayesian Learning

Fu, Maozhong; Li, Yuhan; Deng, Zhenmiao; Sun, Haixin; Christensen, Mads Graesboll

Published in:
IEEE Transactions on Vehicular Technology

DOI (link to publication from Publisher):
10.1109/TVT.2022.3180328

Publication date:
2022

Document Version
Accepted author manuscript, peer reviewed version

High-Resolution and Accurate RV Map Estimation by Spare Bayesian Learning

Maozhong Fu, Yuhan Li, Zhenmiao Deng, *Member, IEEE*, Haixin Sun, *Member, IEEE*, and Mads Græsbøll Christensen, *Senior Member, IEEE*

***Abstract*—Range-velocity (RV) map (also called the range-Doppler map) is used in radar to detect targets and estimate the range and velocity of the targets. The conventional range-Doppler processing has its limits in attaining a high-resolution RV map with few samples. Moreover, the conventional range-Doppler processing may cause severe range migration problems and bias in the range estimation. In this paper, we propose to attain a high-resolution and accurate RV map with the sparse Bayesian learning (SBL) framework. Unlike the existing works that use the discrete Fourier transform to build the dictionary for sparse representation, we build a dictionary from a model of the wide-band frequency-modulated continuous-wave (FMCW) radar to avoid the model mismatch problem. This dictionary allows for the effective decomposition of the signal and the full utilization of the structure of the signal. In addition, based on the fast marginal likelihood maximization, we also propose a fast method to reduce the computational burden. Simulations show that the proposed method and the proposed fast method are superior in terms of resolution, accuracy, and maximum unambiguous velocity compared with the existing methods.**

***Index Terms*—frequency-modulated continuous-wave (FMCW) radar, sparse Bayesian learning, range-Doppler coupling, range-velocity map**

I. Introduction

FREQUENCY modulated continuous wave (FMCW) radars have attracted wide attention in civilian applications in recent years [1], [2], [3], [4], [5], [6]. Compared with other sensors, such as cameras, LiDARs, and ultrasonics, radars show their advantage in the all-weather and day-and-night capability. The range resolution is a critical performance criterion for a radar system. FMCW is one of the most widely used waveforms in existing radar systems for the reason that it can achieve high range resolution with low hardware requirements.

FMCW radars operate by a conjugate mixing of the transmitted chirp signal with the received returns to generate the beat signal whose frequency is proportional to the target range [7]. A frequency estimation technique, like the digital Fourier transform (DFT), is typically used to estimate the range. The target velocity is calculated from multiple sweeps by the Doppler processing which also typically uses the DFT to measure the Doppler shift. Thus, a range-velocity (RV) map (also known as the range-Doppler spectrum or range-Doppler image) can be obtained for target detection and tracking with a two-dimensional (2-D) DFT operation. However, owing to the limited sample size, the DFT-based methods suffer from poor resolution and high side-lobe [8].

In civilian radar applications, the target number is typically far smaller than the sample number, and a target only occupies a few RV cells such that the RV map is sparse. Therefore, the RV map estimation problem can be cast as a sparse representation problem. By exploiting the underlying sparsity, the sparse representation techniques can realize super-resolution with a limited sample number [9]. In general, attaining the sparse representation requires resolving an ill-posed optimization problem. ℓ_p-norm ($p \leq 1$) regularization is widely incorporated to achieve sparsity in these cases [10]. However, the choice of regularization parameter can significantly affect the accuracy of the result and the optimal value often depends on unknown signal characteristics.

Sparse Bayesian learning (SBL) is another popular technique to solve the sparse representation problem [11], [12], [13], [14], [15], [16], [17]. Unlike the ℓ_p-norm-based methods, SBL regularizes the solution space of the ill-posed optimization problem in a data-dependent way without the user input [18], [19]. Specifically, SBL uses a two-layer hierarchical prior model to promote sparsity, and the hyper-parameters of the model are iteratively learned from the data [20].

In RV map estimation, the SBL-based methods have been demonstrated to be superior to the conventional methods in terms of accuracy, resolution, and interference mitigation [21], [22], [23], [24]. A key issue in the sparse representation is to choose a suitable dictionary to decompose the signal. Unfortunately, the existing methods often build the dictionaries directly from the DFT, which is only suitable for narrow-band radars and slow-speed targets. With the increase of the bandwidth and the appearance of high-speed targets in civilian applications, the model mismatch problem will occur and lead to range bias and resolution degradation in RV map estimation.

In order to attain a high-resolution and accurate RV map, we propose an RV map estimation method under the SBL framework. The model mismatch problem is mitigated by adopting a sparsifying dictionary. Due to many radar applications being time-critical, we also propose a fast method based on the fast marginal likelihood maximization algorithm [25]. Furthermore, to improve the robustness and convergence rate

Maozhong Fu is with the School of Informatics, Xiamen University, Xiamen 361005, China, e-mail: maozhongfu@gmail.com.

Yuhan Li is with the School of Informatics, Xiamen University, Xiamen 361005, China, e-mail: YuhanLi1995@hotmail.com.

Zhenmiao Deng is with the School of Electronics and Communication Engineering, Sun Yat-sen University, Guangzhou 510275, China, e-mail: dengzhm7@sysu.edu.cn.

Haixin Sun is with the School of Informatics, Xiamen University, Xiamen 361005, China, e-mail: hxsun@xmu.edu.cn.

Mads Græsbøll Christensen is with the Audio Analysis Lab, Department of Architecture, Design and Media Technology, Aalborg University, Aalborg 9000, Denmark, e-mail: mgc@create.aau.dk.

of the fast method, the noise variance estimator in [13] is adopted.

The rest of this paper is organized as follows. The signal model of the FMCW radar is briefly introduced in Section II. The proposed SBL-based method for RV map estimation is presented in Section III. The theoretical analysis on the difference of the choice of the dictionary between the proposed method and the existing method is presented in Section IV. Fast implementation of the proposed method is derived in Section V. Simulations and experiments are carried out in Section VII to show the effectiveness of the proposed method. Finally, the conclusions are drawn in Section VIII.

Throughout this paper, we use the following notation: matrices and vectors are represented by uppercase and lowercase letters, respectively. For a vector $\mathbf{a}$, $\mathbf{a}_n$ denotes the n-th entry of $\mathbf{a}$. For a sequence $\mathcal{S}$ and a vector $\mathbf{a}$, $\mathbf{a}_{\mathcal{S}}$ is a $K \times 1$ vector consisting of the K entries of $\mathbf{a}$ indexed by $\mathcal{S}$. For a matrix $\mathbf{A}$, $\mathbf{A}_{m,n}$ denotes the (m,n)-th entry of $\mathbf{A}$. For a sequence $\mathcal{S}$ and a matrix $\mathbf{A}$, $\mathbf{A}_{\mathcal{S}}$ is a $N \times K$ matrix consisting of the K columns of $\mathbf{A}$ indexed by $\mathcal{S}$. $\mathbf{I}^{(N)}$ denotes the $N \times N$ identity matrix. $\mathbf{i}^{(N)}$ denotes the $N \times 1$ vector of ones. $\mathbf{o}^{(N)}$ denotes the $N \times 1$ vector of zeros. $(\cdot)^*$, $(\cdot)^{\mathrm{T}}$, and $(\cdot)^{\mathrm{H}}$ denote the conjugate, transpose, and Hermitian transpose operators, respectively. $(\cdot)^+$ denotes the Moore-Penrose pseudo-inverse operator. $\odot$ denotes the Hadamard product. $\%$ denotes the modulo operator. $\lfloor \cdot \rfloor$ and $\lceil \cdot \rceil$ denote the floor and ceiling operators, respectively. $\mathrm{vec}(\cdot)$ denotes the column-major vectorization operation that reshapes a $M \times N$ matrix into a $MN \times 1$ vector. $\mathrm{vec}^{-1}_{M \times N}(\cdot)$ denotes the inverse vectorization operation that reshapes a $MN \times 1$ vector into a $M \times N$ matrix. $\mathrm{diag}(\mathbf{a})$ denotes a diagonal matrix whose diagonal entries are the elements of the vector $\mathbf{a}$. $\mathrm{tr}(\cdot)$ denotes the trace of a matrix. The ℓ_p-norm of a vector $\mathbf{a} \in \mathbb{C}^N$ is defined as $\|\mathbf{a}\|_p = \left(\sum_{n=1}^{N} |x_n|^p\right)^{1/p}$.

II. Signal Model and Problem Formulation

The overview of a FMCW radar system is depicted in Fig. 1. The radar system transmits a train of FMCW pulses for range-velocity map estimation. The waveform of the transmitted FMCW signal can be represented as

$$s_{\text{tx}}(t) = \mathrm{rect}\left(\frac{t}{T}\right) \exp(j2\pi(f_0 t + 0.5kt^2)) \quad \text{for } t \in [0, T_r), \tag{1}$$

where T is the sweep duration, f_0 is the starting frequency, $k = B/T$ is the sweep slope, B is the sweep bandwidth, T_r is the sweep repetition interval, and

$$\mathrm{rect}(u) = \begin{cases} 1 & \text{for } 0 \le u < 1 \\ 0 & \text{otherwise} \end{cases} \tag{2}$$

is the rectangle function. The signal emitted from the transmit (Tx) antenna hits a target and is reflected back to the receive (Rx) antenna. The m-th ($m = 0, \ldots, N_p - 1$) received signal contains the round-trip delay and can be expressed as

$$s_{\text{rx}}(t) = \alpha s(t - mT_r - \tau(t)) \quad \text{for } t \in [mT_r, (m+1)T_r), \tag{3}$$

where α is complex amplitude of the target and $\tau(t)$ is the time-dependent round-trip delay. When the coherent processing interval (CPI) length ($N_p \times T_r$) is short, the target velocity is assumed to be constant during one CPI. Therefore, (3) can be approximated by

$$s_{\text{rx}}(t) = \alpha s(t - mT_r - 2(r + vt)/c) \quad \text{for } t \in [mT_r, (m+1)T_r), \tag{4}$$

where r is the radial range between target and radar when $t = 0$, v is the radial velocity of the target, and c is the speed of light. The m-th received signal is conjugately mixed with the transmitted signal and fed into the low-pass filter (LPF) to produce a low-frequency beat signal

$$\begin{aligned} s_{\text{beat}}(t) &= s^*_{\text{rx}}(t) s_{\text{tx}}(t - mT_r) \\ &= \alpha \Pi(t) \exp\Bigg(j\frac{4\pi}{c}\Bigg(f_0 + k\frac{r}{c} \\ &\quad + k\frac{v}{c}t + k(t - mT_r)\Bigg)(r + vt)\Bigg) \\ &\quad \text{for } t \in [mT_r, (m+1)T_r), \end{aligned} \tag{5}$$

where

$$\begin{aligned} \Pi(t) &= \mathrm{rect}\left(\frac{t - mT_r}{T}\right) \mathrm{rect}\left(\frac{t - mT_r - \frac{2(r+vt)}{c}}{T}\right) \\ &= \mathrm{rect}\left(\frac{t - mT_r - \frac{2(r+vmT_r)}{c-2v}}{T - \frac{2(r+vmT_r)}{c-2v}}\right) \\ &\quad \text{for } t \in [mT_r, (m+1)T_r) \end{aligned} \tag{6}$$

is a rectangular window depending on the range and velocity of the target. Since $v \ll c$, $r \ll Tc$, and $B \ll f_0$ hold for typical automotive applications, we have $k\frac{r}{c} \ll f_0$ and $k\frac{v}{c}t \ll kt$. For example, when using a radar system with $T = 1$ ms, $f_0 = 77$ GHz, and $B = 300$ MHz to deal with a target with $r = 200$ m and $v = 50$ m/s, the term $k\frac{r}{c}$ is 2.6×10^6 times less than f_0 and the term $k\frac{v}{c}t$ is 1.667×10^7 times less than kt. Thus, after neglecting $k\frac{r}{c}$ and $k\frac{v}{c}t$, (5) can be simplified as

$$s_{\text{beat}}(t) \approx \alpha \Pi(t) \exp\left(j\frac{4\pi}{c}\left(f_0 + k(t - mT_r)\right)(r + vt)\right) \quad \text{for } t \in [mT_r, (m+1)T_r). \tag{7}$$

To mitigate the leakage from the Tx antenna to the Rx antenna, the beginning part of the beat signal is discarded. This operation is equivalent to virtually multiplying a smaller rectangular window with the beat signal,

$$\begin{aligned} s_{\text{trim}}(t) &= s_{\text{beat}}(t) \,\mathrm{rect}\left(\frac{t - mT_r - \tau_{\max}}{T - \tau_{\max}}\right) \\ &= \alpha \,\mathrm{rect}\left(\frac{t - mT_r - \tau_{\max}}{T - \tau_{\max}}\right) \\ &\quad \times \exp\left(j\frac{4\pi}{c}(f_0 + k(t - mT_r))(r + vt)\right) \\ &\quad \text{for } t \in [mT_r, (m+1)T_r), \end{aligned} \tag{8}$$

where $\tau_{\max}$ is the maximum of $\frac{2(r+vmT_r)}{c-2v}$ for all possible range and velocity. After passing through the analog-to-digital converter (ADC), the discretized measurements of the m-th pulse

This article has been accepted for publication in IEEE Transactions on Vehicular Technology. This is the author's version which has not been fully edited and content may change prior to final publication. Citation information: DOI 10.1109/TVT.2022.3180328

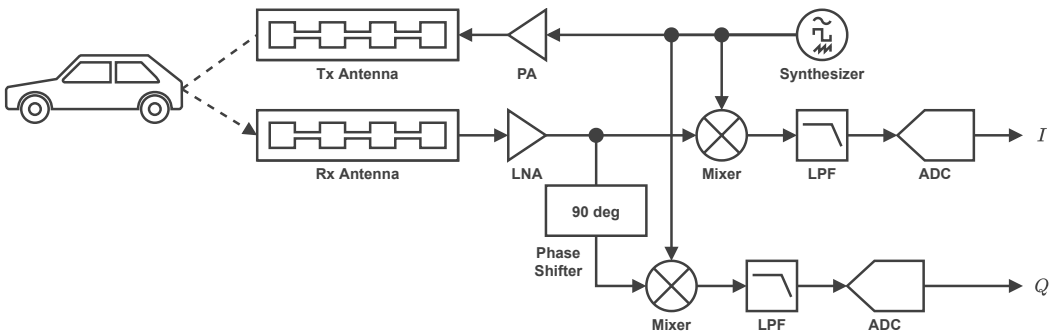

Fig. 1: Simplified block diagram of a FMCW radar system.

can be obtained. Define the slow-time $t_{\text{slow}} = mT_r$ and fast-time $t_{\text{fast}} = t - t_{\text{slow}} = nT_s$, where T_s is the sample interval, $n = n_0, \ldots, N_s - 1$ is the fast-time index, $n_0 = \lceil f_s \tau_{\max} \rceil$, $f_s = 1/T_s$ is the sample rate, and $N_s = \lceil f_s(T - \tau_{\max}) \rceil$ is the sample number in the sampling window. The measurements of the whole N_p pulses can be expressed with the two time indices as

$$y(m,n) = \alpha \exp\left(j\frac{4\pi}{c}(f_0 + knT_s)(r + v(mT_r + nT_s))\right) + w(m,n), \tag{9}$$

where the pulse index m is also denoted as the slow-time index and $w(m,n)$ is the noise.

The region of the interested range-velocity (RV) map can be divided into a $N_r \times N_v$ grid, where N_r and N_v are the numbers of the range and velocity cells, respectively. Obviously, the RV map can be represented by the complex amplitudes on the grid. Define $x(i_r, i_v)$ as the complex amplitude of the target located at (i_r, i_v), where $i_r \in [0, N_r - 1]$ and $i_v \in [0, N_v - 1]$ are the indexes of the range and velocity cells, respectively. And if there is no target located at (i_r, i_v), $x(i_r, i_v) = 0$. The measurements in (9) can represented with $\{x(i_r, i_v)\}_{i_r \in [0, N_r - 1], i_v \in [0, N_v - 1]}$ as

$$y(m,n) = \sum_{i_r=0}^{N_r-1} \sum_{i_v=0}^{N_v-1} x(i_r, i_v)\varphi(i_r, i_v, m, n) + w(m,n), \tag{10}$$

where

$$\varphi(i_r, i_v, m, n) = \exp\left(j\frac{4\pi}{c}(f_0 + knT_s)(i_r\Delta_r + i_v\Delta_v(mT_r + nT_s))\right), \tag{11}$$

Δ_r is the size of the range cell, and Δ_v is the size of the velocity cell. By vectorizing the $y(m,n)$, the vector $\mathbf{y} \in \mathbb{C}^{N \times 1}$ $(N = N_p N_s)$ can be obtained as

$$\mathbf{y} = \text{vec}\left(\begin{bmatrix} y(0,n_0) & \cdots & y(N_p-1,n_0) \\ \vdots & \ddots & \vdots \\ y(0,N_s-1) & \cdots & y(N_p-1,N_s-1) \end{bmatrix}\right). \tag{12}$$

Similarly, the noise vector $\mathbf{w} \in \mathbb{C}^{N \times 1}$ is given by

$$\mathbf{w} = \text{vec}\left(\begin{bmatrix} w(0,n_0) & \cdots & w(N_p-1,n_0) \\ \vdots & \ddots & \vdots \\ w(0,N_s-1) & \cdots & w(N_p-1,N_s-1) \end{bmatrix}\right). \tag{13}$$

The complex amplitudes which consist of the RV map can be represented as a matrix $\mathbf{X} \in \mathbb{C}^{N_r \times N_v}$,

$$\mathbf{X} = \begin{bmatrix} x^{(0,0)} & \cdots & x^{(0,N_v-1)} \\ \vdots & \ddots & \vdots \\ x^{(N_r-1,0)} & \cdots & x^{(N_r-1,N_v-1)} \end{bmatrix}. \tag{14}$$

The vectorized RV map is $\mathbf{x} \in \mathbb{C}^{M \times 1}$ $(M = N_r N_v)$,

$$\mathbf{x} = \text{vec}(\mathbf{X}). \tag{15}$$

The phase term in (10) can be represented with a matrix $\mathbf{\Phi} \in \mathbb{C}^{N \times M}$,

$$\mathbf{\Phi}_{i,l} = \varphi(l\%N_s, \lfloor i/N_s + 0.5 \rfloor, i\%N_r, \lfloor i/N_r + 0.5 \rfloor). \tag{16}$$

With (12)~(16), (10) can be rewritten in matrix form

$$\mathbf{y} = \mathbf{\Phi}\mathbf{x} + \mathbf{w}. \tag{17}$$

In typical automotive applications, only a few targets are in the radar beam, and a target only occupies a few RV cells. Obviously, $\mathbf{x}$ is sparse and has only a few non-zero entries. Therefore, the RV map estimation problem can be converted to a sparse recovery problem where $\mathbf{y}$ is the measurements, $\mathbf{\Phi}$ is the redundant dictionary, $\mathbf{x}$ is the sparse representation, and $\mathbf{w}$ is the noise.

III. Range-Velocity Map Estimation by Spare Bayesian Learning

The system of linear equations in (17) typically is underdetermined. The regularization-based methods can effectively solve this system of linear equations by setting a user-defined regularization parameter. SBL avoids the choice of user parameters and estimates $\mathbf{x}$ by solving a probabilistic parameter estimation problem.

SBL regards $\mathbf{x}$ as a vector of stochastic variables. Thus, the estimate of $\mathbf{x}$ can be found by maximizing the posterior which can be given via Bayes's theorem as

$$p(\mathbf{x}|\mathbf{y}) = \frac{p(\mathbf{y}|\mathbf{x})p(\mathbf{x})}{p(\mathbf{y})}, \tag{18}$$

where $p(\mathbf{x}|\mathbf{y})$ is the posterior, $p(\mathbf{y}|\mathbf{x})$ is the likelihood, $p(\mathbf{y})$ is the evidence, and $p(\mathbf{x})$ is the prior. To enforce the sparsity of $\mathbf{x}$, SBL adopts the zero-mean complex Gaussian distribution as the prior [12], i.e.,

$$p(\mathbf{x};\boldsymbol{\gamma}) = \mathcal{CN}(\mathbf{x}|\mathbf{0},\boldsymbol{\Gamma}), \tag{19}$$

where $\boldsymbol{\Gamma} = \text{diag}(\boldsymbol{\gamma})$ and $\boldsymbol{\gamma} = [\gamma_1, \gamma_2, \ldots, \gamma_M]^{\text{T}}$ is the vector of the hyper-parameters. The hyper-parameter $\boldsymbol{\gamma}_i$ controls the strength of the prior over the i-th component of $\mathbf{x}$. When $\boldsymbol{\gamma}_i = 0$, then p-th component of $\mathbf{x}$ equals 0 with probability 1, which imposes sparsity constraints on $\mathbf{x}$.

We assume that $\mathbf{w}$ follows a zero-mean complex Gaussian distribution, i.e., $p(\mathbf{w}) = \mathcal{CN}(\mathbf{w}|\mathbf{0}, \lambda\mathbf{I}^{(M)})$. Therefore, the likelihood, i.e., the conditional probability density function (PDF) for $\mathbf{y}$ given $\mathbf{x}$ is

$$p(\mathbf{y}|\mathbf{x};\lambda) = \mathcal{CN}(\mathbf{y}|\boldsymbol{\Phi}\mathbf{x}, \lambda\mathbf{I}^{(M)}). \tag{20}$$

The evidence, which is the product of the prior and the likelihood integrated over $\mathbf{x}$, can be expressed as

$$p(\mathbf{y};\boldsymbol{\gamma},\lambda) = \int p(\mathbf{y}|\mathbf{x};\lambda)p(\mathbf{x};\boldsymbol{\gamma})d\mathbf{x} = \mathcal{CN}(\mathbf{y}|\mathbf{0},\mathbf{C}) \tag{21}$$

where

$$\mathbf{C} = \mathbb{E}(\mathbf{y}\mathbf{y}^{\text{H}}) = \lambda\mathbf{I}^{(N)} + \boldsymbol{\Phi}\boldsymbol{\Gamma}\boldsymbol{\Phi}^{\text{H}} \tag{22}$$

is the covariance of $\mathbf{y}$. Substituting (19) and (20) into (18), the posterior PDF of $\mathbf{x}$ conditioned on $\boldsymbol{\gamma}$ and λ can be expressed as

$$p(\mathbf{x}|\mathbf{y};\boldsymbol{\gamma},\lambda) = \frac{p(\mathbf{y}|\mathbf{x};\lambda)p(\mathbf{x};\boldsymbol{\gamma})}{p(\mathbf{y};\boldsymbol{\gamma},\lambda)} \propto \mathcal{CN}(\boldsymbol{\mu},\boldsymbol{\Sigma}), \tag{23}$$

where the posterior mean $\boldsymbol{\mu}$ and covariance $\boldsymbol{\Sigma}$ are

$$\boldsymbol{\mu} = \boldsymbol{\Gamma}\boldsymbol{\Phi}^{\text{H}}\mathbf{C}^{-1}\mathbf{y} \tag{24}$$

and

$$\boldsymbol{\Sigma} = \boldsymbol{\Gamma} - \boldsymbol{\Gamma}\boldsymbol{\Phi}^{\text{H}}\mathbf{C}\boldsymbol{\Phi}\boldsymbol{\Gamma}, \tag{25}$$

respectively. Since the posterior follows a complex Gaussian distribution, the maximum-a-posteriori (MAP) estimate of $\mathbf{x}$ is the posterior mean. Therefore, given the estimates of $\boldsymbol{\Gamma}$ and λ, the MAP estimate of $\mathbf{x}$ is

$$\mathbf{x}_{\text{MAP}} = \boldsymbol{\mu}. \tag{26}$$

After performing inverse vectorization on $\mathbf{x}_{\text{MAP}}$, the matrix of the reconstructed RV map can be obtained as

$$\mathbf{X}_{\text{MAP}} = \text{vec}^{-1}_{N_r \times N_v}(\mathbf{x}_{\text{MAP}}). \tag{27}$$

The unknown hyper-parameters $\boldsymbol{\gamma}$ and noise variance λ can be estimated from the evidence as described next. Taking the logarithm of (21) and keeping only the terms that depend on $\boldsymbol{\gamma}$ and λ, the log marginal likelihood can be obtained as

$$\mathcal{L}(\boldsymbol{\gamma},\lambda) = -\log|\mathbf{C}| - \mathbf{y}^{\text{H}}\mathbf{C}^{-1}\mathbf{y}. \tag{28}$$

Taking the derivative of (28) with respect to $\boldsymbol{\gamma}$ and forcing the result to zero, a fixed-point-based learning rule for $\boldsymbol{\gamma}$ can be obtained as [13]

$$\boldsymbol{\gamma} \leftarrow \frac{\|\boldsymbol{\mu}\|_2}{\sqrt{((\boldsymbol{\Phi}^{\text{H}}\mathbf{C}^{-1}) \odot \boldsymbol{\Phi}^{\text{H}})\mathbf{i}^{(N)}}}. \tag{29}$$

Algorithm 1 RV map estimation by SBL.

Input: $\boldsymbol{\Phi} \in \mathbb{C}^{N\times M}$, $\mathbf{y} \in \mathbb{C}^{N\times 1}$, K, ϵ_{stop}, N_{iter}
Output: $\mathbf{X}_{\text{MAP}} \in \mathbb{C}^{N_r \times N_v}$

$\lambda \leftarrow 1$, $\boldsymbol{\gamma} \leftarrow \mathbf{i}^{(M)}$, $\epsilon \leftarrow \infty$, $n_{\text{iter}} \leftarrow 1$, $\overline{\boldsymbol{\gamma}} \leftarrow \mathbf{o}^{(M)}$
while $\epsilon < \epsilon_{\text{stop}}$ and $n_{\text{iter}} \leq N_{\text{iter}}$ **do**
  $\mathbf{C} \leftarrow \lambda\mathbf{I}^{(N)} + \boldsymbol{\Phi}\boldsymbol{\Gamma}\boldsymbol{\Phi}^{\text{H}}$ ▷ (22)
  $\boldsymbol{\mu} \leftarrow \boldsymbol{\Gamma}\boldsymbol{\Phi}^{\text{H}}\mathbf{C}^{-1}\mathbf{y}$ ▷ (24)
  $\boldsymbol{\gamma} \leftarrow \frac{\|\boldsymbol{\mu}\|_2}{\sqrt{((\boldsymbol{\Phi}^{\text{H}}\mathbf{C}^{-1})\odot\boldsymbol{\Phi}^{\text{H}})\mathbf{i}^{(N)}}}$ ▷ (29)
  $\mathcal{Q} \leftarrow \{q \in \mathbb{N} | \gamma_q \geq \gamma^{(K)}\}$ ▷ (31)
  $\lambda \leftarrow \frac{1}{N-K}\text{tr}\left(\left(\mathbf{I}^{(N)} - \boldsymbol{\Phi}_{\mathcal{Q}}\boldsymbol{\Phi}_{\mathcal{Q}}^{+}\right)\mathbf{S}_y\right)$ ▷ (30)
  $\epsilon \leftarrow \frac{\|\boldsymbol{\gamma}-\overline{\boldsymbol{\gamma}}\|_1}{\|\boldsymbol{\gamma}\|_1}$ ▷ (32)
  $\overline{\boldsymbol{\gamma}} \leftarrow \boldsymbol{\gamma}$
  $n_{\text{iter}} \leftarrow n_{\text{iter}} + 1$
end while
$\mathbf{X}_{\text{MAP}} \leftarrow \text{vec}^{-1}_{N_r\times N_v}(\boldsymbol{\mu})$ ▷ (27)

With the updated $\boldsymbol{\gamma}$, a stochastic-maximum-likelihood-based learning rule of λ is given by [13]

$$\lambda \leftarrow \frac{1}{N-K}\text{tr}\left(\left(\mathbf{I}^{(N)} - \boldsymbol{\Phi}_{\mathcal{Q}}\boldsymbol{\Phi}_{\mathcal{Q}}^{+}\right)\mathbf{S}_y\right), \tag{30}$$

where $\mathbf{S}_y = \mathbf{y}\mathbf{y}^{\text{H}}$ is the covariance matrix of the measurements,

$$\mathcal{Q} = \langle q : q \in \mathbb{N} | \boldsymbol{\gamma}_q \geq \boldsymbol{\gamma}^{(k)} \rangle \tag{31}$$

is the monotonic increasing sequence of the indies indicating the position of the K largest elements of $\boldsymbol{\gamma}$, and $\boldsymbol{\gamma}^{(K)}$ is the K-th largest elements of $\boldsymbol{\gamma}$.

The updates for $\boldsymbol{\gamma}$ and λ should be carried out iteratively until convergence. The convergence criterion of the iteration is defined as

$$\epsilon = \frac{\|\boldsymbol{\gamma} - \overline{\boldsymbol{\gamma}}\|_1}{\|\boldsymbol{\gamma}\|_1}, \tag{32}$$

where $\overline{\boldsymbol{\gamma}}$ is the vector of the estimated hyper-parameters in the previous iteration. The algorithm terminates when ϵ is smaller than a specified value ϵ_{stop} or the iteration number is larger than the maximum number of iterations N_{iter}. It can be noted that most of the elements of $\boldsymbol{\gamma}$ may be close to 0 when convergence is reached, which indirectly drives most of the elements of $\mathbf{x}_{\text{MAP}}$ to be 0. Algorithm 1 summarizes the procedures of the proposed range-velocity map estimation method.

IV. Dictionary for Range-Velocity Map Estimation

The choice of a suitable redundant dictionary is crucial for sparse representation. Here, we analyze the difference between the proposed method and the existing methods in choosing redundant dictionaries for RV map estimation.

The conventional radar signal processing simplifies (9) for RV map estimation using the discrete Fourier transform (DFT). The simplified measurements can be expressed as

$$y(m,n) \approx \alpha' \exp\left(j\frac{4\pi}{c}knT_s r\right)\exp\left(j\frac{4\pi}{c}f_0 vmT_r\right) + w(m,n), \tag{33}$$

where $\alpha' = \alpha \exp\left(j\frac{4\pi}{c} f_0 r\right)$ is a complex constant. It can be noted that the simplified signal is the product of two sinusoidal terms $\exp\left(j\frac{4\pi}{c} knT_s r\right)$ and $\exp\left(j\frac{4\pi}{c} f_0 vmT_r\right)$. Therefore, the RV map can be obtained by taking a 2-dimensional (2-D) DFT on $y(m,n)$ along n and m [26]. This operation is called the range-Doppler processing for RV map estimation. The simplified signal model adopted by the range-Doppler processing mainly has the following drawbacks:

1) Resolution degradation for wide-band radars and high-speed targets. By comparing (9) and (33), it can be noted that the term $\exp\left(j\frac{4\pi}{c} knT_s vmT_r\right)$ causing the range-velocity coupling in the slow-time (also known as the range migration phenomenon) is neglected. This term is related to the bandwidth, the CPI length, and the target velocity. For a wide-band radar and a high-speed target, this term can degrade the resolution significantly [7].
2) Bias in the range domain for high-speed targets. It can also be noted that term $\exp\left(j\frac{4\pi}{c}(f_0 + knT_s)vnT_s\right)$ in (33) representing a phase rotation in the fast-time is neglected. For a typical civilian radar system, we have $\exp\left(j\frac{4\pi}{c}(f_0 + knT_s)vnT_s\right) \approx \exp\left(j\frac{4\pi}{c} f_0 vnT_s\right)$ which is the range-velocity coupling in the fast-time. According to the frequency-shifting property of the Fourier transform, performing the DFT on $\exp\left(j\frac{4\pi}{c} f_0 vnT_s\right)$ will cause a velocity-dependent shift in the range domain, which means the RV map obtained with the range-Doppler processing is biased in the range domain. For high-speed targets, the range bias in the RV map may be too high to be accepted.
3) Limited measurable range of velocity. The RV map estimation with the range-Doppler processing is equivalent to sampling the slow-time at $2c/(4T_r f_0)$. It is known that for a complex signal sampled at f_s, the frequency range is limited to $(-0.5f_s, 0.5f_s]$. Thus, the measured velocity is limited to $\left(-c/(4T_r f_0), c/(4T_r f_0)\right]$. In fact, the information of the target velocity is only derived from the term $\exp\left(j\frac{4\pi}{c} f_0 vmT_r\right)$ in (33) for the range-Doppler processing. However, the information of the target velocity also lies in the two coupling terms which are not utilized by the range-Doppler processing.

As analyzed above, the range-Doppler processing is based on the narrow-band and slow-speed targets model, which is mismatched with the wide-band waveform and high-speed targets in modern civilian applications. Some existing works exploit the DFT matrix to construct the redundant dictionaries for RV map estimation with SBL techniques [21], [22]. Since their redundant dictionaries do not resolve this model mismatch problem, they suffer from the same drawbacks as the range-Doppler processing.

To address the model mismatch problem, we propose to integrate the two coupling terms into the redundant dictionary for RV map estimation. Under the framework of SBL, the coupling terms can be utilized to attain RV maps with higher resolution, higher accuracy, and a larger measurable range of velocity.

V. Fast Implementation of the Proposed Method

Computational efficiency is important for civilian radars and many other applications. Hence, we here present a fast method based on the fast marginal likelihood maximization [25], [27].

Assuming that we are interested in a single hyper-parameter $\boldsymbol{\gamma}_i$ ($i \in [1, \ldots, M]$). Equation (22) can be rewritten as

$$\begin{aligned}\mathbf{C} &= \boldsymbol{\gamma}_i \boldsymbol{\Phi}_i \boldsymbol{\Phi}_i^{\mathrm{H}} + \lambda \mathbf{I}^{(N)} + \sum_{l=1, l\neq i}^{M} \boldsymbol{\gamma}_l \boldsymbol{\Phi}_l \boldsymbol{\Phi}_l^{\mathrm{H}} \\ &= \boldsymbol{\gamma}_i \boldsymbol{\Phi}_i \boldsymbol{\Phi}_i^{\mathrm{H}} + \mathbf{C}_{-i}, \end{aligned} \tag{34}$$

where $\mathbf{C}_{-i}$ is $\mathbf{C}$ with the contribution of $\boldsymbol{\Phi}_i$ is removed. Substituting (34) into (22) and using the Woodbury matrix identity and the matrix determinant lemma, we have

$$\begin{aligned}\mathcal{L}(\boldsymbol{\gamma}, \lambda) = &- \log |\mathbf{C}_{-i}| - \mathbf{y}^{\mathrm{H}} \mathbf{C}_{-i}^{-1} \mathbf{y} \\ &- \log(1 + \boldsymbol{\gamma}_i s_i) + \frac{q_i^* q_i \boldsymbol{\gamma}_i}{1 + \boldsymbol{\gamma}_i s_i}, \end{aligned} \tag{35}$$

where

$$s_i = \boldsymbol{\Phi}_i^{\mathrm{H}} \mathbf{C}_{-i}^{-1} \boldsymbol{\Phi}_i \tag{36}$$

and

$$q_i = \boldsymbol{\Phi}_i^{\mathrm{H}} \mathbf{C}_{-i}^{-1} \mathbf{y}. \tag{37}$$

Forcing $\frac{\partial \mathcal{L}(\boldsymbol{\gamma}, \lambda)}{\partial \boldsymbol{\gamma}_i}$ to zero shows that $\mathcal{L}(\boldsymbol{\gamma}, \lambda)$ has a unique maximum at

$$\boldsymbol{\gamma}_i' = \frac{q_i^* q_i - s_i}{s_i^2}. \tag{38}$$

In practice, it is more efficient to compute s_i and q_i as [25]:

$$s_i = \frac{S_i}{1 - \boldsymbol{\gamma}_i S_i} \tag{39}$$

and

$$q_i = \frac{Q_i}{1 - \boldsymbol{\gamma}_i S_i}, \tag{40}$$

where

$$S_i = \boldsymbol{\Phi}_i^{\mathrm{H}} \mathbf{B} \boldsymbol{\Phi}_i - \boldsymbol{\Phi}_i^{\mathrm{H}} \mathbf{B} \boldsymbol{\Phi} \boldsymbol{\Sigma} \boldsymbol{\Phi}^{\mathrm{H}} \mathbf{B} \boldsymbol{\Phi}_i, \tag{41}$$

$$Q_i = \boldsymbol{\Phi}_i^{\mathrm{H}} \mathbf{B} \mathbf{y} - \boldsymbol{\Phi}_i^{\mathrm{H}} \mathbf{B} \boldsymbol{\Phi} \boldsymbol{\Sigma} \boldsymbol{\Phi}^{\mathrm{H}} \mathbf{B} \mathbf{y}, \tag{42}$$

and $\mathbf{B} = \lambda^{-1} \mathbf{I}^{(N)}$.

For different values of $\boldsymbol{\gamma}_i$ in (38), different actions may be taken. Define $\mathcal{I}$ as the monotonic increasing sequence of the indices of the hyper-parameters used in marginal likelihood maximization. $\mathcal{I}$ is empty at the start of the algorithm.

When $\boldsymbol{\gamma}_i > 0$, $\boldsymbol{\gamma}_i$ is a valid hyper-parameter. If i is not in $\mathcal{I}$, add i into $\mathcal{I}$. The change of $\mathcal{L}(\boldsymbol{\gamma}, \lambda)$ before and after the addition operation can be calculated efficiently as

$$\Delta_i = \frac{Q_i Q_i^*}{S_i} + \log \frac{S_i}{Q_i Q_i^*} - 1. \tag{43}$$

And if i is already in $\mathcal{I}$, we re-estimate $\boldsymbol{\gamma}_i$. The corresponding change of $\mathcal{L}(\boldsymbol{\gamma}, \lambda)$ can be expressed as

$$\Delta_i = \frac{Q_i Q_i^*}{S_i + (\boldsymbol{\gamma}_i' - \boldsymbol{\gamma}_i)^{-1}} - \log(1 + (\boldsymbol{\gamma}_i' - \boldsymbol{\gamma}_i) S_i). \tag{44}$$

When $\boldsymbol{\gamma}_i < 0$, $\boldsymbol{\gamma}_i$ conflicts with the adopted prior and should be excluded from the marginal likelihood maximization. When $\boldsymbol{\gamma}_i = 0$, $\boldsymbol{\gamma}_i$ has no contribution to the marginal likelihood maximization and should also be excluded. In both cases,

TABLE I: Complexity Analysis of the Proposed Method

Operation	Complexity
Multiplication Between a $N \times M$ Matrix and a $M \times M$ Matrix	$\mathcal{O}(NM^2)$
Multiplication Between a $N \times M$ Matrix and a $M \times N$ Matrix	$\mathcal{O}(N^2M)$
Multiplication Between a $M \times N$ Matrix and a $N \times N$ Matrix	$\mathcal{O}(N^2M)$
Addition/Subtraction Between $N \times N$ Matrices	$\mathcal{O}(N^2)$
Element-Wise Product Between $N \times N$ Matrices	$\mathcal{O}(N^2)$
Calculation of the Matrix Inverse of a $N \times N$ Matrix	$\mathcal{O}(N^3)$
Calculation of the Moore-Penrose Pseudo-Inverse of a $K \times K$ Matrix	$\mathcal{O}(K^3)$
Calculation of the ℓ_p-Norm of a $M \times 1$ vector	$\mathcal{O}(M)$
Finding K Largest Elements in a $M \times 1$ Vector	$\mathcal{O}(M + K\log(M))$

if i is already in $\mathcal{I}$, delete i from $\mathcal{I}$ and set $\boldsymbol{\gamma}_i = 0$. The corresponding change of $\mathcal{L}(\boldsymbol{\gamma}, \lambda)$ is

$$\Delta_i = \frac{Q_i Q_i^*}{S_i - (\boldsymbol{\gamma}_i)^{-1}} - \log(1 - \boldsymbol{\gamma}_i S_i). \tag{45}$$

Assume $\mathcal{I}$ has I elements at the current iteration. Typically, I is much smaller than M. Therefore, $\boldsymbol{\Sigma}$ and $\boldsymbol{\mu}$ can be computed efficiently as

$$\boldsymbol{\Sigma} = (\boldsymbol{\Phi}_{\mathcal{I}}^{\mathrm{H}} \mathbf{B} \boldsymbol{\Phi}_{\mathcal{I}} + \mathrm{diag}(\boldsymbol{\gamma}_{\mathcal{I}})^{-1})^{-1} \tag{46}$$

and

$$\boldsymbol{\mu} = \boldsymbol{\Sigma} \boldsymbol{\Phi}_{\mathcal{I}}^{\mathrm{H}} \mathbf{B} \mathbf{y}, \tag{47}$$

which replaces the $N \times N$ matrix inverse operation in (24) with an $I \times I$ one.

Algorithm 2 gives a detailed description of the fast implementation of the proposed range-velocity map estimation method. It can be noted that the fast implementation of the proposed method is based on a greedy-like algorithm. Thus, this fast method is prone to becoming trapped in local minima when $M > N$ [18].

VI. Computational Complexity and Convergence Analysis

As listed in Algorithm 1, the computation of the proposed RV map estimation method mainly consists of several types of operation. The complexity analysis of these operations is shown in Table I. Since $K < N \ll M$ is valid for most applications, the overall computational complexity of the proposed method is $\mathcal{O}(NM^2)$. Similarly, we list the computational complexity of the operations in Algorithm 2 in Table II. It can be noted that the element number of $\mathcal{I}$, i.e., I changes during the iteration. It can also be noted that $I \leq N_{\text{iter}}$ and N_{iter} is usually set to a small number for computational efficiency. Thus, we assume $I \leq N_{\text{iter}} < N$ and $N_{\text{iter}} N < M$. In this case, the overall computational complexity of the proposed fast method is $\mathcal{O}(NM)$.

The convergence of the adopted fixed-point iteration in the proposed method is hard to prove analytically. However, its convergence has been verified by Monte Carlo simulations in [13]. The proposed fast method uses a fast marginal likelihood maximization technology which increases the marginal likelihood at each iteration, therefore it is guaranteed to converge to a local maximum [25].

Algorithm 2 Fast implementation of RV map estimation by SBL.

Input: $\boldsymbol{\Phi} \in \mathbb{C}^{N \times M}$, $\mathbf{y} \in \mathbb{C}^{N \times 1}$, K, ϵ_{stop}, N_{iter}
Output: $\mathbf{X}_{\text{MAP}} \in \mathbb{C}^{N_r \times N_v}$

$\lambda \leftarrow 1$, $\boldsymbol{\gamma} \leftarrow \mathbf{o}^{(M)}$, $\epsilon \leftarrow \infty$, $\mathcal{I} \leftarrow \emptyset$, $n_{\text{iter}} \leftarrow 1$, $\overline{\boldsymbol{\gamma}} \leftarrow \mathbf{o}^{(M)}$
$i \leftarrow \arg\max_{i'}(|(\boldsymbol{\Phi}_{i'})^{\mathrm{H}} \mathbf{Y}|)$, $i' \in [1, M]$
$\mathcal{I} \leftarrow \{i\} \cup \mathcal{I}$
while $\epsilon < \epsilon_{\text{stop}}$ and $n_{\text{iter}} \leq N_{\text{iter}}$ **do**
  $\boldsymbol{\Sigma} \leftarrow (\boldsymbol{\Phi}_{\mathcal{I}}^{\mathrm{H}} \mathbf{B} \boldsymbol{\Phi}_{\mathcal{I}} + \mathrm{diag}(\boldsymbol{\gamma}_{\mathcal{I}})^{-1})^{-1}$ ▷ (46)
  $\boldsymbol{\mu} \leftarrow \boldsymbol{\Sigma} \boldsymbol{\Phi}_{\mathcal{I}}^{\mathrm{H}} \mathbf{B} \mathbf{y}$ ▷ (47)
  for all $i \in [1, M]$ **do**
    $S_i \leftarrow \boldsymbol{\Phi}_i^{\mathrm{H}} \mathbf{B} \boldsymbol{\Phi}_i - \boldsymbol{\Phi}_i^{\mathrm{H}} \mathbf{B} \boldsymbol{\Phi} \boldsymbol{\Sigma} \boldsymbol{\Phi}^{\mathrm{H}} \mathbf{B} \boldsymbol{\Phi}_i$ ▷ (41)
    $Q_i \leftarrow \boldsymbol{\Phi}_i^{\mathrm{H}} \mathbf{B} \mathbf{y} - \boldsymbol{\Phi}_i^{\mathrm{H}} \mathbf{B} \boldsymbol{\Phi} \boldsymbol{\Sigma} \boldsymbol{\Phi}^{\mathrm{H}} \mathbf{B} \mathbf{y}$ ▷ (42)
    $s_i \leftarrow \frac{S_i}{1 - \boldsymbol{\gamma}_i S_i}$ ▷ (39)
    $q_i \leftarrow \frac{Q_i}{1 - \boldsymbol{\gamma}_i S_i}$ ▷ (40)
    $\boldsymbol{\gamma}_i' \leftarrow \frac{q_i^* q_i - s_i}{s_i^2}$ ▷ (38)
    if $\boldsymbol{\gamma}_i' > 0$ and $i \notin \mathcal{I}$ **then**
      $\Delta_i \leftarrow \frac{Q_i Q_i^*}{S_i} + \log \frac{S_i}{Q_i Q_i^*} - 1$ ▷ (43)
    else if $\boldsymbol{\gamma}_i' > 0$ and $i \in \mathcal{I}$ **then**
      $\Delta_i \leftarrow \frac{Q_i Q_i^*}{S_i + (\boldsymbol{\gamma}_i' - \boldsymbol{\gamma}_i)^{-1}} - \log(1 + (\boldsymbol{\gamma}_i' - \boldsymbol{\gamma}_i) S_i)$ ▷ (44)
    else if $\boldsymbol{\gamma}_i' \leq 0$ and $i \in \mathcal{I}$ **then**
      $\Delta_i \leftarrow \frac{Q_i Q_i^*}{S_i - (\boldsymbol{\gamma}_i)^{-1}} - \log(1 - \boldsymbol{\gamma}_i S_i)$ ▷ (45)
    end if
  end for
  $i \leftarrow \arg\max_{i'}(\Delta_{i'})$, $i' \in [1, M]$
  if $\boldsymbol{\gamma}_i' > 0$ and $i \notin \mathcal{I}$ **then**
    $\mathcal{I} \leftarrow \{i\} \cup \mathcal{I}$, $\boldsymbol{\gamma}_i \leftarrow \boldsymbol{\gamma}_i'$ ▷ Update $\boldsymbol{\gamma}$ with $\boldsymbol{\gamma}_i'$
  else if $\boldsymbol{\gamma}_i' > 0$ and $i \in \mathcal{I}$ **then**
    $\boldsymbol{\gamma}_i \leftarrow \boldsymbol{\gamma}_i'$ ▷ Add $\boldsymbol{\gamma}_i'$ to $\boldsymbol{\gamma}$
  else if $\boldsymbol{\gamma}_i' \leq 0$ and $i \in \mathcal{I}$ **then**
    $\mathcal{I} \leftarrow \mathcal{I} \setminus \{i\}$, $\boldsymbol{\gamma}_i \leftarrow 0$ ▷ Delete $\boldsymbol{\gamma}_i$ from $\boldsymbol{\gamma}$
  end if
  $\mathcal{Q} \leftarrow \{q \in \mathbb{N} | \gamma_q \geq \gamma^{(K)}\}$ ▷ (31)
  $\lambda \leftarrow \frac{1}{N-K} \mathrm{tr}\left(\left(\mathbf{I}^{(N)} - \boldsymbol{\Phi}_{\mathcal{Q}} \boldsymbol{\Phi}_{\mathcal{Q}}^{+}\right) \mathbf{S}_y\right)$ ▷ (30)
  $\epsilon \leftarrow \frac{\|\boldsymbol{\gamma} - \overline{\boldsymbol{\gamma}}\|_1}{\|\boldsymbol{\gamma}\|_1}$ ▷ (32)
  $\overline{\boldsymbol{\gamma}} \leftarrow \boldsymbol{\gamma}$
  $n_{\text{iter}} \leftarrow n_{\text{iter}} + 1$
end while
$\mathbf{X}_{\text{MAP}} \leftarrow \mathrm{vec}^{-1}_{N_r \times N_v}(\boldsymbol{\mu})$ ▷ (27)

VII. Simulations and Experiments

In this section, we present several simulations to investigate the performance of the proposed method. The simulations are all carried out in MATLAB using computer-generated data. The signal-to-noise ratio (SNR) of a target is defined as SNR $= |\alpha|^2 / \lambda$. The parameters of the simulations are in Table III, if not specified otherwise. The notation (r, v)

TABLE II: Complexity Analysis of the Proposed Fast Method

Operation	Complexity
Multiplication Between a $1\times N$ Matrix and a $N\times N$ Matrix	$\mathcal{O}(N^2)$
Multiplication Between a $1\times N$ Matrix and a $N\times M$ Matrix	$\mathcal{O}(NM)$
Multiplication Between a $1\times M$ Matrix and a $M\times N$ Matrix	$\mathcal{O}(NM)$
Multiplication Between a $1\times N$ Matrix and a $N\times 1$ Matrix	$\mathcal{O}(N)$
Multiplication Between a $I\times N$ Matrix and a $N\times N$ Matrix	$\mathcal{O}(IN^2)$
Multiplication Between a $I\times N$ Matrix and a $N\times I$ Matrix	$\mathcal{O}(I^2N)$
Multiplication Between a $I\times I$ Matrix and a $I\times N$ Matrix	$\mathcal{O}(I^2N)$
Multiplication Between a $I\times N$ Matrix and a $N\times 1$ Matrix	$\mathcal{O}(IN)$
Calculation of the Matrix Inverse of a $I\times I$ Matrix	$\mathcal{O}(I^3)$
Addition/Subtraction Between $I\times I$ Matrices	$\mathcal{O}(I^2)$
Addition/Subtraction Between $N\times N$ Matrices	$\mathcal{O}(N^2)$
Calculation of the Moore-Penrose Pseudo-Inverse of a $K\times K$ Matrix	$\mathcal{O}(K^3)$
Calculation of the ℓ_p-Norm of a $M\times 1$ vector	$\mathcal{O}(M)$
Finding the Maximum of a $M\times 1$ Vector	$\mathcal{O}(M)$
Finding K Largest Elements of a $M\times 1$ Vector	$\mathcal{O}(M+K\log(M))$

is used to denote the target's position in the range-velocity domain. The units of range and velocity are m and $\mathrm{m/s}$, respectively. The amplitudes of all estimated RV maps are normalized to 1 for ease of comparison. For convenience, the RV map estimation methods, including the proposed method, the proposed fast method, the conventional range-Doppler processing, and the BSBL-based method [21] are denoted by SBL-RV, FSBL-RV, DFT-RV, and BSBL-RV, respectively. In addition, considering that the ℓ_1 regularization techniques are widely used for sparse representation recovery, we combine the LASSO method provided in [28] with the same dictionary used by SBL-RV and FSBL-RV for the RV map estimation and denote this method by LASSO-RV. The grid spacing of the dictionaries is set according to half of the conventional resolutions (the range resolution is $C/(2B)$ and the velocity resolution is $c/(2f_0T_rN_p)$ [26]) to make a balance between the RV map size and the RV cell size for a better presentation. The block size which is an input parameter of BSBL-RV is set to 3. The maximum iteration number of SBL-RV and BSBL-RV are both set to 500. Since FSBL-RV uses a greed-like algorithm and does not require a large iteration number to achieve optimal performance, its iteration number is set to 50. For the simulations, the regularization parameter of LASSO-RV is chosen by minimizing the mean-square-error (MSE) between the true value and the recovered RV map at $\mathrm{SNR}=10$ dB. The stop criterion of SBL-RV, FSBL-RV, and BSBL-RV are all set to 1×10^{-6}. In practice, the results of SBL-based methods are not sensitive to the choice of K [29]. Thus, K of SBL-RV and FSBL-RV are both set to 1.

TABLE III: Simulation Parameters

Symbol	Parameter	Value
f_0	Starting Frequency	$24\,\mathrm{GHz}$
B	Sweep Bandwidth	$300\,\mathrm{MHz}$
T	Sweep Duration	$533\,\mu\mathrm{s}$
T_r	Sweep Repetition Interval	$533\,\mu\mathrm{s}$
$\tau_{\max}$	Maximum Possible Delay	$21\,\mu\mathrm{s}$
N_p	Pulse Number	16
λ	Noise Variance	1
SNR	Signal-to-Noise Ratio	$10\,\mathrm{dB}$

A. Maximum Unambiguous Velocity

In this simulation, we compare the maximum unambiguous velocity of the RV map estimation methods. To compare the maximum unambiguous velocity, we consider three targets are located at positions $(7.7586, 8.7339)$, $(7.7586, 0)$, and $(7.7586, -8.7339)$ in the RV domain, respectively. It can be noted that the velocities of the 1st target and the 3rd target are both beyond the maximum unambiguous velocity of DFT-RV and BSBL-RV. In this case, the measured velocities of these two high-speed targets will be folded into values within $\big(-c/(4T_rf_0), c/(4T_rf_0)\big] = \big(-5.859, 5.859\big]$ $\mathrm{m/s}$. This phenomenon is called the velocity/Doppler ambiguity problem[30]. The white circles indicate the ground truth of the positions of the targets in the RV map. As illustrated in Fig. 2(a)~(b), the velocity ambiguity problem occurs on the two high-speed targets. As expected, the velocities of two high-speed targets are folded into 2.8749 $\mathrm{m/s}$ and 2.8749 $\mathrm{m/s}$, respectively, which are far from the ground truth. DFT-RV and BSBL-RV are suffered from the Doppler ambiguity problem. By contrast, LASSO-RV, SBL-RV, and FSBL-RV are all free from the velocity ambiguity problem since the coupling terms are included in the redundant dictionary. As shown in Fig. 2(c)~(e), all the targets match the ground truth well.

B. Accuracy

In this simulation, we compare the accuracy of the RV map estimation methods. Three targets are located in the RV domain with positions $(7.2414, 5.1312)$, $(7.2414, 0)$, and $(7.2414, -5.1312)$, respectively, is considered in the simulated scene. Fig. 3 shows the RV map estimation results for accuracy comparison. It can be observed from Fig. 3(c)~(e) that the results of LASSO-RV, SBL-RV, and FSBL-RV all match the ground truth well, whereas the result of BSBL-RV shows deviation from the ground truth for the targets with non-zero velocity in Fig. 3(b). From Fig. 3(a), it can be observed that the result of DFT-RV also matches the ground truth. However, this is due to the fact that the range bias of DFT-RV is smaller than the resolution. For the high-speed targets, the range bias of DFT-RV can be larger than the resolution, which can be observed in Fig. 2(a). These results suggest that SBL-RV and FSBL-RV have an advantage over the existing methods that

This article has been accepted for publication in IEEE Transactions on Vehicular Technology. This is the author's version which has not been fully edited and content may change prior to final publication. Citation information: DOI 10.1109/TVT.2022.3180328

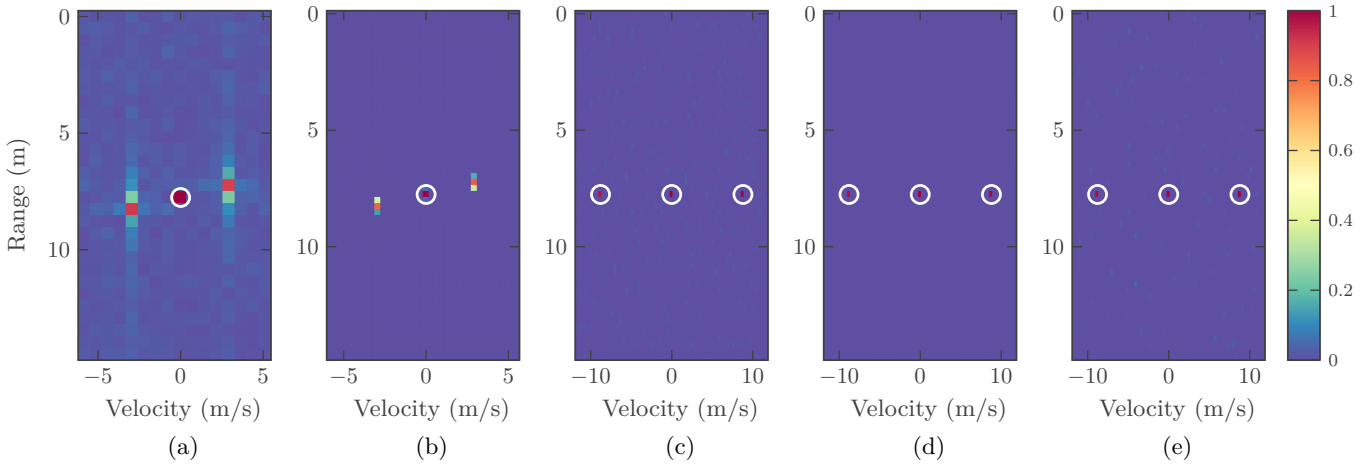

Fig. 2: Maximum unambiguous velocity comparison. (a) DFT-RV. (b) BSBL-RV. (c) LASSO-RV. (d) SBL-RV. (e) FSBL-RV.

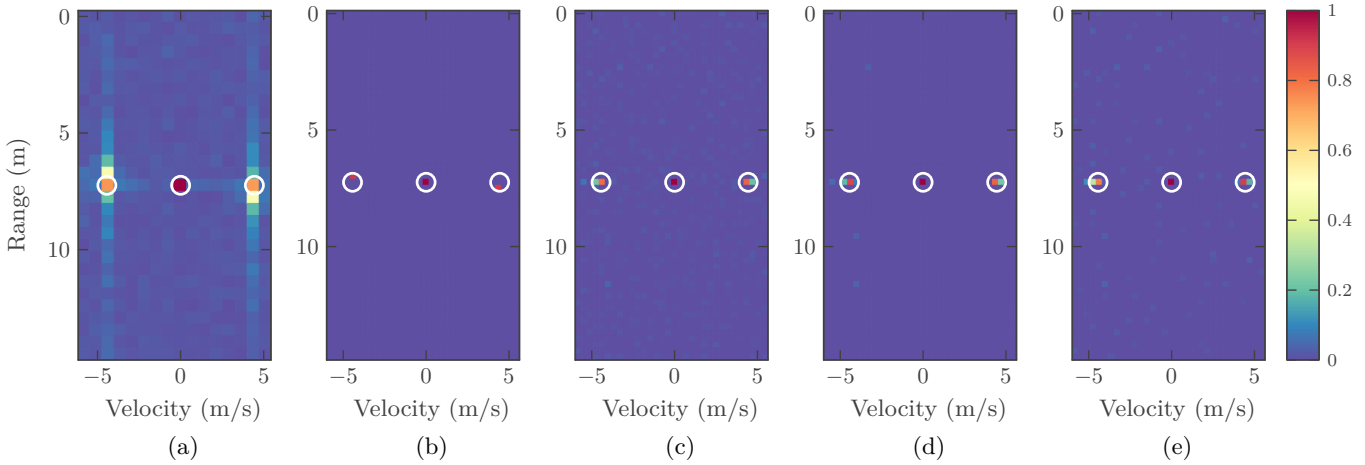

Fig. 3: Accuracy comparison. (a) DFT-RV. (b) BSBL-RV. (c) LASSO-RV. (d) SBL-RV. (e) FSBL-RV.

ignores the coupling terms in terms of the accuracy of the RV map estimation.

C. Resolution

In this simulation, we investigate the resolution performance of the proposed methods, i.e., SBL-RV and FSBL-RV. Two closed distributed targets with positions $(2.526, 0)$ and $(2.842, 0)$ are considered in the RV domain. It is known that the grid spacing of the dictionary affects the resolution of the result for a sparse recovery problem. Thus, the grid spacing of dictionaries is set to $1/5$ of the conventional resolutions for a better resolution performance. Since the range-velocity cell is small in this case, we only show part of the obtained RV map for better presentation. Fig. 4 shows the comparison result of the resolution performance. As it can be deduced from Fig. 4(a), these two closed distributed targets can not be identified by DFT-RV. These two targets are merged in the same range-velocity cell. BSBL-RV also fails to identify these two targets, which can be observed in Fig. 4(b). As for LASSO-RV, it shows a significant degradation in resolution performance in Fig. 4(c). From Fig. 4(d)~(e), it can be seen that these two targets can be identified in the RV maps obtained with SBL-RV and FSBL-RV. Evidently, SBL-RV and FSBL-RV both have a higher resolution than DFT-RV, BSBL-RV, and LASSO-RV.

As mentioned in Section IV, the RV coupling in the slow-time may greatly degrade the resolution for the high-speed targets. Therefore, a simulated scene where two high-speed targets are in the RV domain with positions $(2.526, 49)$ and $(2.842, 49)$ are considered. Fig. 5 presents the results of the resolution comparison for the high-speed targets. It can be seen from Fig. 5(a) that the energy of the two targets leaks into the adjacent RV cells due to the RV coupling in the slow-time, which makes it harder to detect the two targets for DFT-RV. Similarly, it can be observed from Fig. 5(b) that the energy of the two targets spread over more RV cells for BSBL-RV in the high-speed cases. The result of LASSO-RV in Fig. 5(c) is similar to that in Fig. 4(c), which implies that LASSO-RV is insensitive to the target speed but still can not distinguish the closed distributed targets. By comparing Fig. 4(d)~(e) and Fig. 5(d)~(e), it can be found that SBL-RV and FSBL-RV can provide consistent high-resolution results for both the slow-

This article has been accepted for publication in IEEE Transactions on Vehicular Technology. This is the author's version which has not been fully edited and content may change prior to final publication. Citation information: DOI 10.1109/TVT.2022.3180328

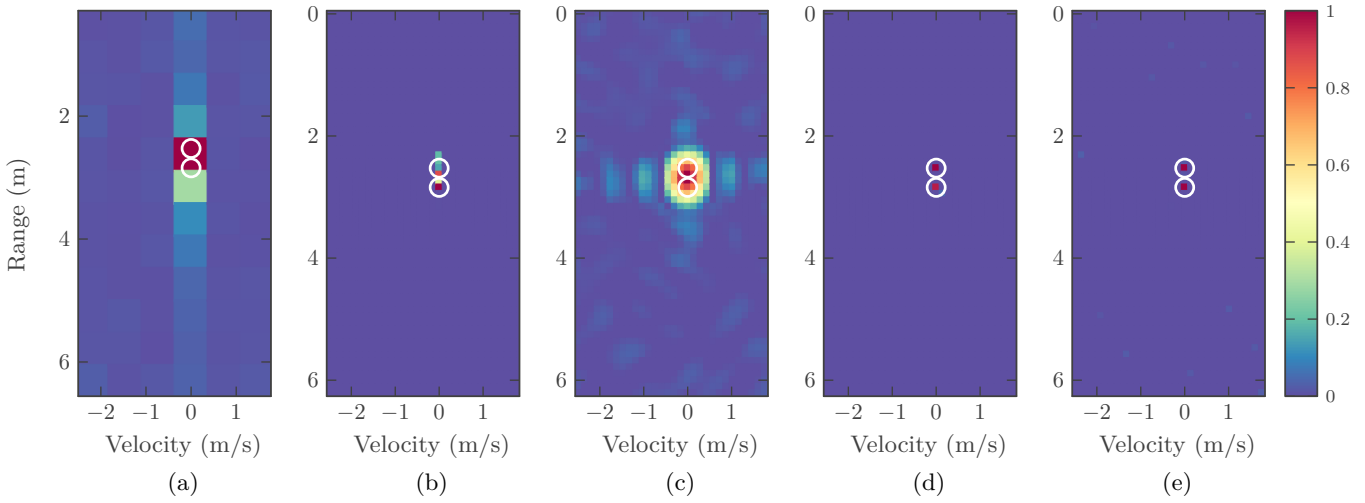

Fig. 4: Resolution comparison for close distributed and slow-speed targets. (a) DFT-RV. (b) BSBL-RV. (c) LASSO-RV. (d) SBL-RV. (e) FSBL-RV.

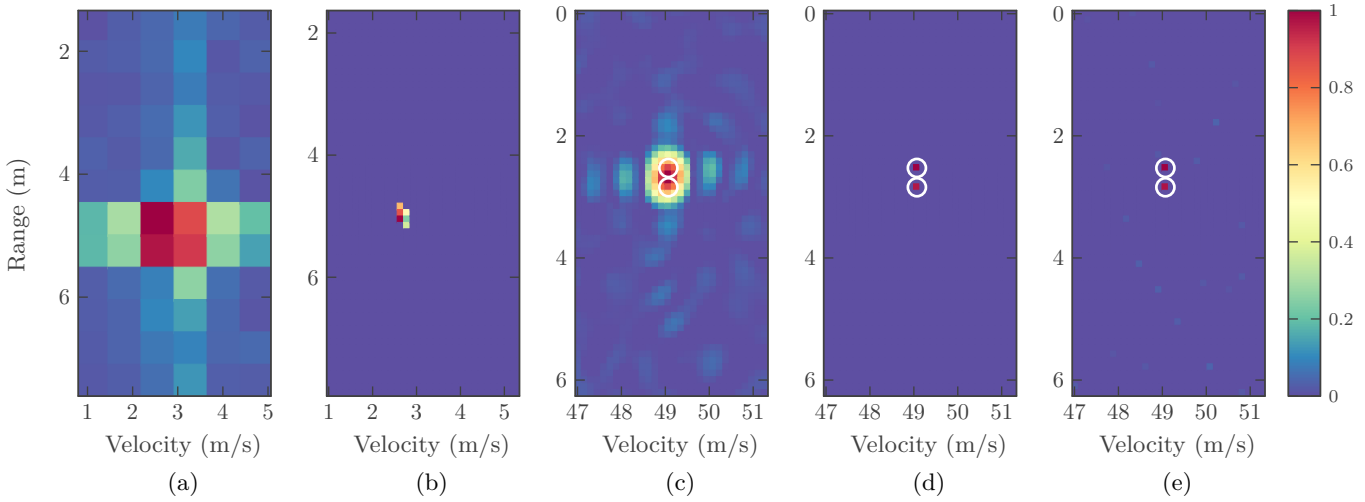

Fig. 5: Resolution comparison for close distributed and high-speed targets. (a) DFT-RV. (b) BSBL-RV. (c) LASSO-RV. (d) SBL-RV. (e) FSBL-RV.

speed and high-speed targets.

As analyzed in Section IV, a larger bandwidth can cause more severe resolution degradation for high-speed targets. Therefore, we increase the bandwidth to $1.5\,\mathrm{GHz}$, while keeping other parameters of the previous simulation unchanged, and show the corresponding results in Fig. 6. As it can be observed from Fig. 5(a)~(b), the resolution performance of DFT-RV and BSBL-RV further degrades for the increased bandwidth. The energy of the two targets leaks into more adjacent RV cells. From Fig. 5(c), it can be seen that LASSO-RV is greatly benefited from the increased bandwidth and can distinguish the two targets in this case. SBL-RV and FSBL-RV retain their high resolution for the increased bandwidth as can be observed in Fig. 5 5(d)~(e).

D. Off-Grid Problems

The proposed method adopts a on-grid assumption on the targets' range and velocity. Since in practice the unknown range and velocity of the targets may not always locate exactly in the RV cells, we investigate the performance of proposed methods in the off-grid cases. Two off-grid targets with $(1.842, 0)$ and $(3.947, 0)$ are considered. From Fig. 7(a)~(c), it can be seen that DFT-RV, BSBL-RV, and LASSO-RV all surfer badly from the off-grid problem. The off-grid problem mainly causes the bias in range and velocity for DFT-RV and significantly deteriorates the resolution performance of BSBL-RV and LASSO-RV. The accuracy of SBL-RV and FSBL-RV also are affected by the off-grid problems. However, from Fig. 7(d)~(e), it can be seen that their resolution deterioration and bias are relatively small and can be ignored in real-world applications.

E. Computation Efficiency

In this simulation, we evaluate the computational efficiency of the proposed methods. A target with position $(2.526, 0)$

This article has been accepted for publication in IEEE Transactions on Vehicular Technology. This is the author's version which has not been fully edited and content may change prior to final publication. Citation information: DOI 10.1109/TVT.2022.3180328

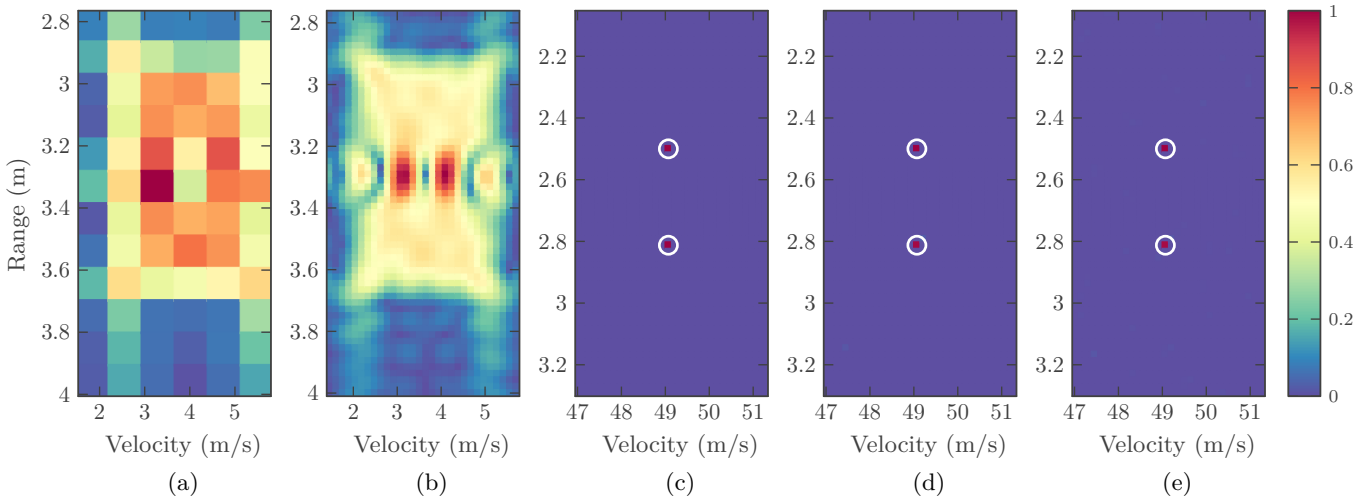

Fig. 6: Resolution comparison for a larger bandwidth. (a) DFT-RV. (b) BSBL-RV. (c) LASSO-RV. (d) SBL-RV. (e) FSBL-RV.

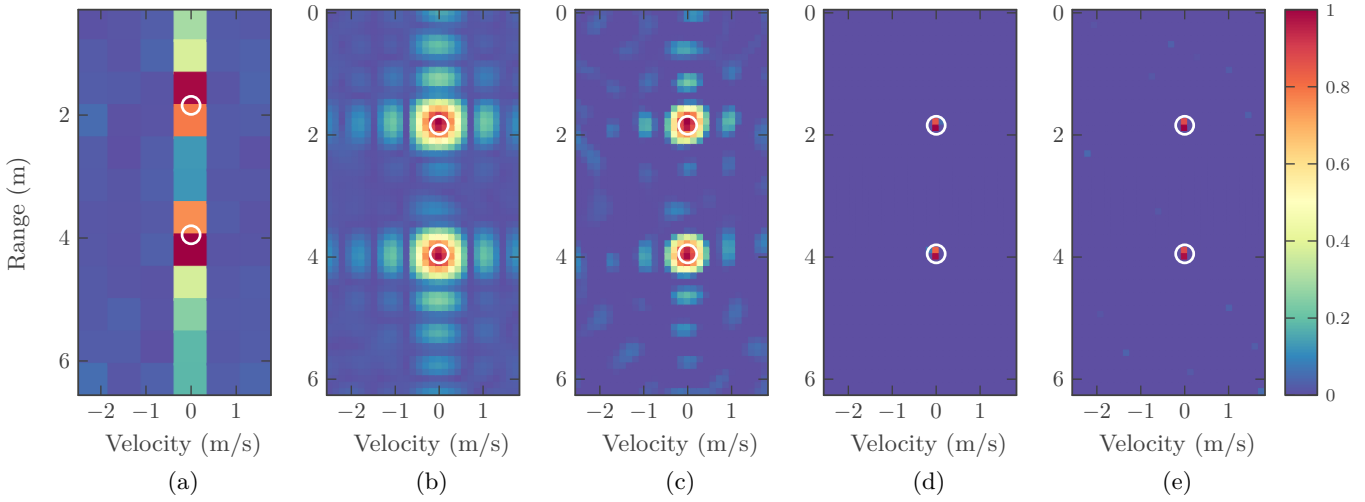

Fig. 7: Resolution comparison for off-grid targets. (a) DFT-RV. (b) BSBL-RV. (c) LASSO-RV. (d) SBL-RV. (e) FSBL-RV.

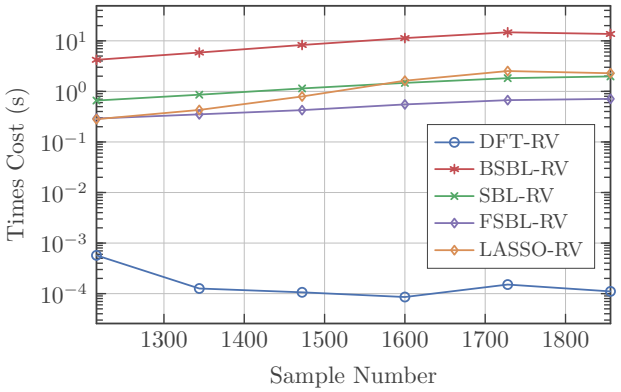

Fig. 8: Time cost comparison.

in the RV domain is simulated. The average time cost of 10 runs of each method is calculated with the various sample number. Fig. 8 presents the results. Some observations can be made. Since DFT-RV can be implemented via a single 2-D fast Fourier transform, it has the lowest computational burden. BSBL-RV is based on the expectation-maximization algorithm, therefore it has the highest computational cost. SBL-RV uses the fixed-point iteration technique to achieve fast convergence, and FSBL-RV adopts a greed-like strategy which has been demonstrated to be fast. Consequently, SBL-RV and FSBL-RV both require much less time cost than BSBL-RV, and FSBL-RV is slightly faster than SBL-RV.

F. Real-World Data Processing

The real-world data are collected by a traffic flow radar. The parameters of the radar system are listed in Table IV. The targets are cars. The clutter from the ground, buildings, and other stationary objects are removed removing the associated components per range bin in range DFT. The grid spacing of the dictionaries is set to $1/3$ of the conventional resolutions. The regularization parameter of LASSO-RV is manually tuned for a good enough result. Fig. 9 shows the results for real-world data processing. It can be seen that BSBL-RV, LASSO-

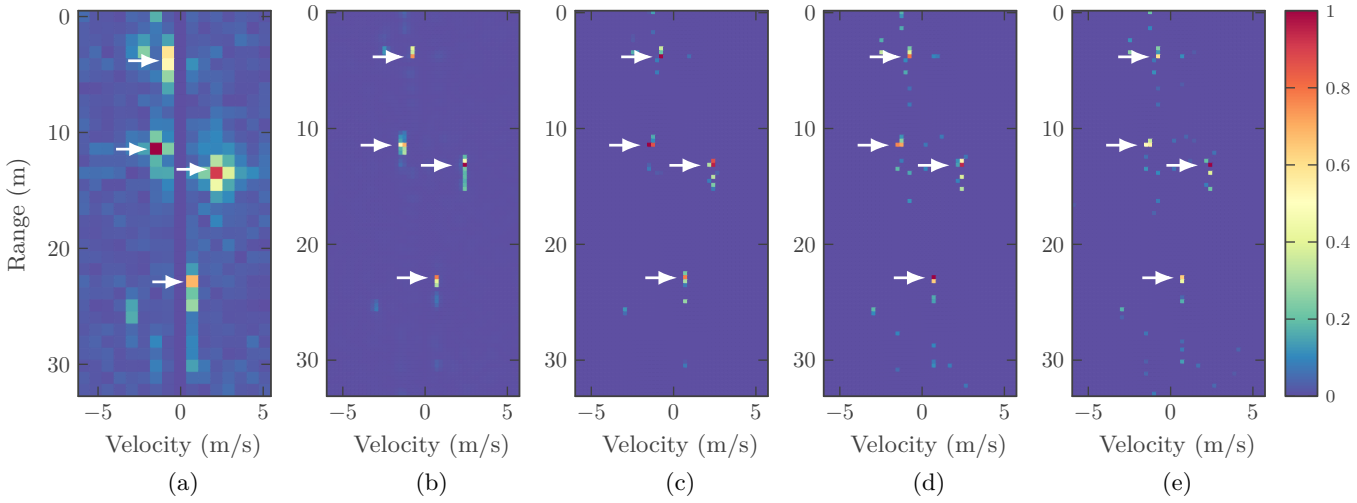

Fig. 9: RV maps obtained with the measured data. (a) DFT-RV. (b) BSBL-RV. (c) LASSO-RV. (d) SBL-RV. (e) FSBL-RV.

TABLE IV: Parameters of the Traffic Flow Radar

Symbol	Parameter	Value
f_0	Starting Frequency	24 GHz
B	Sweep Bandwidth	150 MHz
T	Sweep Duration	533 µs
T_r	Sweep Repetition Interval	533 µs
$\tau_{\max}$	Maximum Possible Delay	21 µs
N_p	Pulse Number	32

RV, SBL-RV, and FSBL-RV all can provide a better resolution than DFT-RV.

VIII. Conclusion

In this paper, we propose a high-resolution and accurate RV map estimation method (called SBL-RV) under the SBL framework. The theoretical analysis of the difference between SBL-RV and the existing methods at choosing the dictionary for sparse representation is carried out. To achieve higher computational efficiency, we also propose a fast method (called FSBL-RV) based on the fast marginal likelihood maximization algorithm. Extensive simulation results are provided to verify the effectiveness of SBL-RV and FSBL-RV. The interesting findings includes:

- SBL-RV and FSBL-RV have a higher resolution than the conventional range-Doppler processing, which makes them more suitable for modern civilian radar applications, such as automotive radar and drone swarm detection.
- SBL-RV and FSBL-RV have an advantage over the existing methods in terms of the accuracy of the RV map. The range bias caused by RV coupling in the fast-time is removed successfully.
- SBL-RV and FSBL-RV can provide an RV map with a higher range of maximum unambiguous velocity, which means that SBL-RV and FSBL-RV are free from the Doppler ambiguity problem.
- SBL-RV and FSBL-RV are less efficient than DFT-RV. Nevertheless, they require much less computation cost than BSBL-RV, which also is based on the SBL framework
- FSBL-RV is more computationally efficient than SBL-RV, but SBL-RV is more robust than FSBL-RV since FSBL-RV is more prone to becoming trapped in local minima than SBL-RV when maximizing the evidence.

Acknowlegment

The authors would like to thank China Scholarship Council (CSC) for the funding support for the first author.

References

[1] S. Lee, J.-Y. Lee, and S.-C. Kim, "Mutual Interference Suppression Using Wavelet Denoising in Automotive FMCW Radar Systems," *IEEE Transactions on Intelligent Transportation Systems*, vol. 22, no. 2, pp. 887–897, Feb. 2021.

[2] F. Uysal, "Phase-Coded FMCW Automotive Radar: System Design and Interference Mitigation," *IEEE Transactions on Vehicular Technology*, vol. 69, no. 1, pp. 270–281, Jan. 2020.

[3] R. Zhang, C. Li, J. Li, and G. Wang, "Range Estimation and Range-Doppler Imaging Using Signed Measurements in LFMCW Radar," *IEEE Transactions on Aerospace and Electronic Systems*, vol. 55, no. 6, pp. 3531–3550, Dec. 2019.

[4] S. Neemat, F. Uysal, O. Krasnov, and A. Yarovoy, "Reconfigurable Range-Doppler Processing and Range Resolution Improvement for FMCW Radar," *IEEE Sensors Journal*, vol. 19, no. 20, pp. 9294–9303, Oct. 2019.

[5] S. Xu and A. Yarovoy, "Joint Features Extraction for Multiple Moving Targets Using (Ultra-)Wideband FMCW Signals in the Presence of Doppler Ambiguity," *IEEE Transactions on Signal Processing*, vol. 68, pp. 6562–6577, 2020.

[6] A. Rawat, S. Dwivedi, S. Srivastava, and A. K. Jagannatham, "RLS-Based Adaptive Time-Varying RCS Estimation and Imaging in MIMO Radar Systems," in *2020 National Conference on Communications (NCC)*. IEEE, 2020, pp. 1–6.

[7] G. Hakobyan and B. Yang, "High-Performance Automotive Radar: A Review of Signal Processing Algorithms and Modulation Schemes," *IEEE Signal Processing Magazine*, vol. 36, no. 5, pp. 32–44, Sep. 2019.

[8] Y.-H. Pan, C.-H. Lin, and T.-S. Lee, "GAN-CRT: A Novel Range-Doppler Estimation Method in Automotive Radar Systems," in *2020 IEEE 91st Vehicular Technology Conference (VTC2020-Spring)*, May 2020, pp. 1–7.

[9] H. H. Zhang and R. S. Chen, "Coherent Processing and Superresolution Technique of Multi-Band Radar Data Based on Fast Sparse Bayesian Learning Algorithm," *IEEE Transactions on Antennas and Propagation*, vol. 62, no. 12, pp. 6217–6227, Dec. 2014.

[10] A. Xenaki, J. Bünsow Boldt, and M. Græsbøll Christensen, "Sound source localization and speech enhancement with sparse Bayesian learning beamforming," *The Journal of the Acoustical Society of America*, vol. 143, no. 6, pp. 3912–3921, Jun. 2018.

[11] A. Tipping and A. Faul, "Analysis of sparse Bayesian learning," *Advances in neural information processing systems*, vol. 14, pp. 383–389, 2002.

[12] D. P. Wipf and B. D. Rao, "An Empirical Bayesian Strategy for Solving the Simultaneous Sparse Approximation Problem," *IEEE Transactions on Signal Processing*, vol. 55, no. 7, pp. 3704–3716, Jul. 2007.

[13] P. Gerstoft, C. F. Mecklenbrauker, A. Xenaki, and S. Nannuru, "Multi-snapshot Sparse Bayesian Learning for DOA," *IEEE Signal Processing Letters*, vol. 23, no. 10, pp. 1469–1473, Oct. 2016.

[14] S. Nannuru, K. L. Gemba, P. Gerstoft, W. S. Hodgkiss, and C. F. Mecklenbräuker, "Sparse Bayesian learning with multiple dictionaries," *Signal Processing*, vol. 159, pp. 159–170, Jun. 2019.

[15] L. Zhao, X. Li, L. Wang, and G. Bi, "Computationally Efficient Wide-Band DOA Estimation Methods Based on Sparse Bayesian Framework," *IEEE Transactions on Vehicular Technology*, vol. 66, no. 12, pp. 11 108–11 121, Dec. 2017.

[16] A. Mishra, N. Yashaswini, and A. K. Jagannatham, "SBL-Based Joint Sparse Channel Estimation and Maximum Likelihood Symbol Detection in OSTBC MIMO-OFDM Systems," *IEEE Transactions on Vehicular Technology*, vol. 67, no. 5, pp. 4220–4232, May 2018.

[17] S. Srivastava, R. K. Singh, A. K. Jagannatham, and L. Hanzo, "Bayesian learning aided sparse channel estimation for orthogonal time frequency space modulated systems," *IEEE transactions on vehicular technology*, vol. 70, no. 8, pp. 8343–8348, 2021.

[18] D. Wipf and S. Nagarajan, "A New View of Automatic Relevance Determination," *Advances in Neural Information Processing Systems*, vol. 20, pp. 1625–1632, 2007.

[19] K. L. Gemba, S. Nannuru, P. Gerstoft, and W. S. Hodgkiss, "Multi-frequency sparse Bayesian learning for robust matched field processing," *The Journal of the Acoustical Society of America*, vol. 141, no. 5, pp. 3411–3420, May 2017.

[20] N. L. Pedersen, C. Navarro Manchón, M.-A. Badiu, D. Shutin, and B. H. Fleury, "Sparse estimation using Bayesian hierarchical prior modeling for real and complex linear models," *Signal Processing*, vol. 115, pp. 94–109, Oct. 2015.

[21] S. Chen, J. Taghia, U. Kühnau, T. Fei, F. Grünhaupt, and R. Martin, "Automotive Radar Interference Reduction Based on Sparse Bayesian Learning," in *2020 IEEE Radar Conference (RadarConf20)*, Sep. 2020, pp. 1–6.

[22] F. Shen, X. Chen, Y. Liu, G. Zhao, and X. Li, "Range-Doppler Spectrum Estimation via Sparse variational Bayesian approach," *International Journal of Remote Sensing*, vol. 40, no. 2, pp. 794–809, 2019.

[23] A. Filip-Dhaubhadel and D. Shutin, "Long Coherent Integration in Passive Radar Systems Using Super-Resolution Sparse Bayesian Learning," *IEEE Transactions on Aerospace and Electronic Systems*, vol. 57, no. 1, pp. 554–572, Feb. 2021.

[24] H. Liu, B. Jiu, H. Liu, and Z. Bao, "Superresolution ISAR Imaging Based on Sparse Bayesian Learning," *IEEE Transactions on Geoscience and Remote Sensing*, vol. 52, no. 8, pp. 5005–5013, Aug. 2014.

[25] M. E. Tipping and A. C. Faul, "Fast marginal likelihood maximisation for sparse Bayesian models," in *International Workshop on Artificial Intelligence and Statistics*. PMLR, 2003, pp. 276–283.

[26] S. M. Patole, M. Torlak, D. Wang, and M. Ali, "Automotive radars: A review of signal processing techniques," *IEEE Signal Processing Magazine*, vol. 34, no. 2, pp. 22–35, Mar. 2017.

[27] B. Liu, Z. Zhang, G. Xu, H. Fan, and Q. Fu, "Energy efficient telemonitoring of physiological signals via compressed sensing: A fast algorithm and power consumption evaluation," *Biomedical Signal Processing and Control*, vol. 11, pp. 80–88, May 2014.

[28] E. Van Den Berg and M. P. Friedlander, "Probing the Pareto frontier for basis pursuit solutions," *SIAM Journal on Scientific Computing*, vol. 31, no. 2, pp. 890–912, 2009.

[29] K. L. Gemba, S. Nannuru, and P. Gerstoft, "Robust Ocean Acoustic Localization With Sparse Bayesian Learning," *IEEE Journal of Selected Topics in Signal Processing*, vol. 13, no. 1, pp. 49–60, Mar. 2019.

[30] W. Jia, Y. Cao, S. Zhang, and W.-Q. Wang, "Detecting High-Speed Maneuvering Targets by Exploiting Range-Doppler Relationship for LFM Radar," *IEEE Transactions on Vehicular Technology*, vol. 70, no. 3, pp. 2209–2218, Mar. 2021.

Maozhong Fu was born in Fujian, China, in 1990. He received the B.S. and M.S. degrees from Xiamen University (XMU), Xiamen, China, in 2012 and 2015, respectively. He is currently pursuing the Ph.D. degree in communication engineering at XMU. His current research interests include parameter estimation and radar signal processing.

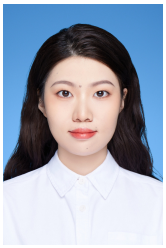

Yuhan Li was born in Fujian, China, in 1995. She received the B.S. degree in communication engineering in 2017 from Nanjing University of Posts and Telecommunications, Nanjing, China. She is currently pursuing the Ph.D. degree in communication engineering at Xiamen University (XMU). Her current research interests include radar imaging and radar signal processing.

Zhenmiao Deng was born in Fujian, China, in 1977. He received the B.S. degree in electronic engineering from the Nanjing University of Aeronautics and Astronautics (NUAA), Nanjing, China, in 1999 and the Ph.D. degree in signal and information processing from the NUAA, Nanjing, China, in 2007. From 2007 to 2009, he was a post-doctor research fellow in the College of Automation Engineering, NUAA, Nanjing, China, working in the field of signal detection and parameter estimation. In 2010, he joined the College of Information Science and Technology, Xiamen University, where he is now a professor. His current research interests include signal detection, parameter estimation, array signal processing, multirate signal processing.

Haixin Sun (Member, IEEE) received the B.S. and M.S. degrees in electronic engineering from the Shandong University of Science and Technology, Shandong, China, in 1999 and 2003, respectively, and the Ph.D. degree in communication engineering from the Institute of Acoustic, Chinese Academy of Science, Shanghai, China, in 2006. He visited the Department of Electrical and Computer Engineering, University of Connecticut, Storrs, CT, USA, from March 2012 to April 2013. He is currently a Professor and a Doctorial Advisor with the School of Informatics, Xiamen University. His current research interests include underwater acoustic communication, and network and signal processing. He is also a member of IEICE. He was awarded the Huawei Fellowship of Xiamen University in 2010, the Faculty of Engineering Excellence Award of Xiamen University, and the Prize of Chinese Army Scientific and Technological in 2017. He has served for journals and conferences as a reviewer.

Mads Græsbøll Christensen (Senior Member, IEEE) received the M.Sc. and Ph.D. degrees from Aalborg University (AAU), Aalborg, Denmark, in 2002 and 2005, respectively. He is currently with the Department of Architecture, Design & Media Technology as Professor in audio processing and is the Head and Founder with the Audio Analysis Lab. He was with the Department of Electronic Systems, AAU, and held visiting positions with Philips Research Labs, ENST, UCSB, and Columbia University, New York, NY, USA. He has authored or coauthored four books and more than 200 papers in peer-reviewed conference proceedings and journals, and he has given multiple tutorials and keynote talks at major intertional conferences. His research interests include audio and acoustic signal processing, such as microphone arrays, noise reduction, signal modeling, speech analysis, audio classification, and audio coding. Dr. Christensen was the recipient of several awards, including best paper awards, the Spar Nord Foundation's Research Prize, a Danish Independent Research Council Young Researcher's Award, Statoil Prize, the EURASIP Early Career Award, and an IEEE SPS Best Paper Award. He was also the recipient of major grants from the Independent Research Fund Denmark, the Villum Foundation, and Innovation Fund Denmark. He is currently the Editor-in-Chief of the EURASIP Journal on Audio, Speech, and Music Processing and as a Senior Area Editor of IEEE SIGNAL PROCESSING LETTERS, and was an Associate Editor for IEEE/ACM IEEE TRANSACTIONS ON A UDIO, SPEECH AND LANGUAGE PROCESSING and IEEE SIGNAL PROCESSING LETTERS. He is a Member of the IEEE Audio and Acoustic Signal Processing Technical Committee and a Founding Member of the EURASIP Special Area Team in Acoustic, Speech and Music Signal Processing. He is a Member of EURASIP and the Danish Academy of Technical Sciences.